International Journal of Structural Stability and Dynamics
Vol. 14, No. 8 (2014) 1440032 (16 pages)

DOI: 10.1142/S021945541440032X

Controlling a Shape Memory Alloy Two-Bar Truss Using Delayed Feedback Method

Aline S. de Paula[*,§], Marcel V. S. dos Santos[*], Marcelo A. Savi[†,¶] and Wallace M. Bessa[‡,‖]

[*]*Universidade de Brasília*
Department of Mechanical Engineering
70.910.900 – Brasília – DF, Brazil

[†]*Universidade Federal do Rio de Janeiro*
COPPE – Department of Mechanical Engineering
21.941.972 – Rio de Janeiro – RJ, P.O. Box 68.503, Brazil

[‡]*Universidade Federal do Rio Grande do Norte*
Department of Mechanical Engineering
59072-970, Natal, RN, Brazil
[§]*alinedepaula@unb.br*
[¶]*savi@mecanica.ufrj.br*
[‖]*wmbessa@ufrnet.br*

Received 1 January 2014
Accepted 11 August 2014
Published 16 October 2014

This work discusses the use of chaos control in smart structures. An archetypal model of a shape memory alloy (SMA) two-bar truss is treated. This system exhibits both constitutive and geometrical nonlinearities presenting a complex nonlinear dynamics response including either the snap-through or the chaotic behaviors. A constitutive model that presents a close agreement with experimental data is employed to describe the themomechanical SMA behavior. A variation of the continuous time-delayed feedback method is employed as a control strategy. This variable structure controller is applied to the stabilization of unstable periodic orbits of the SMA structure avoiding the snap-through behavior.

Keywords: Nonlinear dynamics; von Mises truss; shape memory alloys; pseudoelasticity; chaos control; bifurcation control.

1. Introduction

Chaos control is based on the richness of chaotic behavior and may be understood as the use of tiny perturbations for the stabilization of unstable periodic orbits (UPOs) embedded in chaotic attractors. This procedure makes chaotic behavior to be

[§,‖]Corresponding authors.

desirable in a variety of applications, since one of these UPOs can provide better performance than others in a particular situation. Chaos control methods have being used for different purposes that include either the stabilization of UPOs or bifurcation control.[1,2]

Structural systems are important applications where this kind of idea can be employed. Bifurcation control can be used to avoid undesirable behaviors, and also can promote vibration reduction. Archetypal models are usually employed in order to investigate the general aspects of the structural dynamics, providing a global comprehension of the system behavior. The two-bar truss is one of these archetypal models used to analyze the stability aspects of structures. This kind of system allows one to analyze bifurcation scenarios related to stability changes associated with different characteristics of buckling behavior.[3]

One of the remarkable characteristics of the two-bar truss is the snap-through behavior where, for a given load level, two displacement configurations are possible. Therefore, if the structure is loaded with a monotonically increasing force, the displacement path may jump from one configuration to another. Literature related to stability analysis of structures treats the snap-through and the post-buckling behavior in trusses,[4,5] cylindrical shells,[6,7] thin films,[8] and laminated composites failures.[9]

Snap-through behavior is a classical geometrical nonlinearity. The combination of geometrical and constitutive nonlinearities may increase even more the complex nonlinear dynamics of this kind of system. The combination of geometrical and constitutive nonlinearities was previously addressed by treating the elasto-plastic behavior.[10] Savi *et al.*[11] and Savi and Nogueira[12] analyzed two-bar truss built with shape memory alloys (SMAs) elements. Bessa *et al.*[13] investigated the control of the SMA truss using a slide mode controller.

Shape memory alloys belong to the class of smart materials being used in different kinds of applications.[14–16] Among different thermomechanical behaviors, SMAs present pseudoelastic and shape memory effects that are both associated with solid phase transformations. The pseudoelastic behavior is characterized by complete strain recovery accompanied by large hysteresis in a loading–unloading cycle. The shape memory effect, on the other hand, is characterized by residual strains imposed by a mechanical loading that can be completely recovered by a subsequent thermal loading.

This work deals with the application of chaos control in an SMA two-bar truss. This system has a complex dynamic response and can easily reach a chaotic behavior.[11,12] A constitutive model that presents close agreement with experimental data is employed in order to describe the SMA thermomechanical behavior.[17] A variation of the time-delayed feedback (TDF) method is employed to stabilize unstable periodic orbits (UPOs) embedded in chaotic attractors. Bifurcation control is also of concern showing an interesting potential application of the controller. Besides, it should be highlighted that the vibration reduction can avoid

snap-through behavior. Numerical simulations show that a time-delayed feedback approach can successfully control the structure behavior.

2. Mathematical Modeling and Control Method

Archetypal models are usually employed to investigate the general aspects of complex system dynamics. A plane two-bar truss formed by two identical bars that present only vertical, symmetrical motions, may be employed to investigate the analysis of adaptive trusses with shape memory alloy actuators. The thermomechanical behavior of the SMA is described by assuming a homogeneous phase transformation through the truss. Therefore, constitutive modeling assumes a single-point description and the resulting discrete dynamical system is essentially one-dimensional. Figure 1 shows the two-bar truss formed by two identical bars, both making an angle φ with a horizontal line, and free to rotate around their supports and at the joint. The structure's mass is lumped at the node, and only vertical, symmetrical motions of the truss are considered, being denoted by X. Under these assumptions, the structure is divided into segments without mass, connected by nodes with lumped mass, m. A pseudoelastic two-bar truss is of concern where two identical shape memory alloy elements are considered, represented by bars having length l and cross section area A. The critical Euler load of each bar is assumed to be sufficiently large so that buckling does not occur. Moreover, gravity effect is neglected. In addition, control action is provided by a horizontal displacement denoted by D in Fig. 1.

The balance of momentum is expressed through the following equation of motion, where a linear viscous damping, represented by a coefficient c, is included in the formulation,

$$-2F\sin\varphi - c\dot{X} + P = m\ddot{X}, \tag{1}$$

where F is the force on each bar, P is an external force, $\dot{X}$ and $\ddot{X}$ represent, respectively, the first and second time derivative of X.

The description of force F is related to the SMA thermomechanical behavior and it is assumed that phase transformations are homogeneous through the truss. There

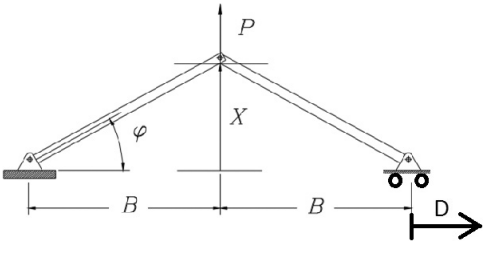

Fig. 1. Two-bar truss (von Mises truss).

are different ways to describe the SMA behavior and here, a constitutive model with internal variables previously discussed in different references[17–23] is employed.

2.1. *Constitutive equations*

Shape memory alloys have a complex thermomechanical behavior associated with solid phase transformations. In essence, SMA has two phases: austenite and martensite. Austenite is stable at high temperatures and stress-free state. On the other hand, martensite is stable at low temperatures and stress-free state. In addition, martensitic phase has variants induced by stress field. Therefore, SMA thermomechanical behavior can be understood by considering macroscopic phases: austenitic phase, A; twinned martensite, M, induced by temperature; detwinned martensitic phases induced by tensile stress, $M+$, or by compressive stress, $M-$.

Here, the thermomechanical description of SMAs employs the constitutive model proposed by Paiva *et al.*[17] In brief, this model considers the following state variables: strain (ε), temperature (T), and three volume fractions of the material phases — β_1 is associated with tensile detwinned martensite ($M+$), β_2 is related to compressive detwinned martensite ($M-$), β_3 represents austenite (A). Actually, it is considered a fourth phase, β_4, related to twinned martensite (M), but it can be expressed from phase coexistence condition ($\beta_4 = 1 - \beta_1 + \beta_2 + \beta_3$). Under these assumptions, it is possible to obtain a complete set of constitutive equations that describes the thermomechanical behavior of SMAs as follows:

$$\sigma = E\varepsilon + [\alpha + E\alpha_h](\beta_2 - \beta_1) - \Omega(T - T_0), \tag{2}$$

$$\dot{\beta}_1 = \frac{1}{\eta}\{\alpha\varepsilon + \Lambda + [2\alpha_h\alpha + E\alpha_h^2](\beta_2 - \beta_1) + \alpha_h[E\varepsilon - \Omega(T - T_0)] - \partial_1 J_\pi\} + \partial_1 J_\chi, \tag{3}$$

$$\dot{\beta}_2 = \frac{1}{\eta}\{-\alpha\varepsilon + \Lambda - [2\alpha_h\alpha + E\alpha_h^2](\beta_2 - \beta_1) - \alpha_h[E\varepsilon - \Omega(T - T_0)] - \partial_2 J_\pi\} + \partial_2 J_\chi, \tag{4}$$

$$\dot{\beta}_3 = \frac{1}{\eta}\left\{-\frac{1}{2}(E_A - E_M)[\varepsilon + \alpha_h(\beta_2 - \beta_1)]^2 + \Lambda_3 + (\Omega_A - \Omega_M)(T - T_0)[\varepsilon + \alpha_h(\beta_2 - \beta_1)] - \partial_3 J_\pi\right\} + \partial_3 J_\chi, \tag{5}$$

where σ is the uniaxial stress, $E = E_M + \beta_3(E_A - E_M)$ is the elastic modulus while $\Omega = \Omega_M + \beta_3(\Omega_A - \Omega_M)$ is related to the thermal expansion coefficient. Note that subscripts "A" and "M" refer, respectively, to austenitic and martensitic phases. Moreover, parameters $\Lambda = \Lambda(T)$ and $\Lambda_3 = \Lambda_3(T)$ are associated with phase transformations stress levels. Parameter α_h controls the horizontal width of the stress–strain hysteresis loop, while α promotes vertical hysteresis loop control on stress–strain curves.

Concerning the parameters definition, temperature dependent relations are adopted for Λ and Λ_3 as follows:

$$\Lambda = \begin{cases} -L_0 + \dfrac{L}{T_M}(T - T_M) & \text{if } T > T_M, \\ -L_0 & \text{if } T \leq T_M, \end{cases} \tag{6a}$$

$$\Lambda_3 = \begin{cases} -L_0^A + \dfrac{L^A}{T_M}(T - T_M) & \text{if } T > T_M, \\ -L_0^A & \text{if } T \leq T_M, \end{cases} \tag{6b}$$

where T_M is the temperature below which the martensitic phase becomes stable in a stress-free state. Besides, L_0, L, L_0^A and L^A are parameters related to critical stress for phase transformation.

With respect to evolution equations of volume fractions, η represents the internal dissipation related to phase transformations. In order to contemplate different characteristics of the kinetics of phase transformation for loading and unloading processes, it is possible to consider different values to the internal dissipation parameter: η^L and η^U during loading and unloading process, respectively.

The terms $\partial_n J_\pi$ and $\partial_n J_\chi$ $(n = 1, 2, 3)$ are sub-differentials of the indicator functions, J_π and J_χ, respectively.[24] They provide a proper description of the model constraints that are essentially related to phase transformations. They can be understood as Lagrange multipliers, being equivalent to projections in volume fractions space. For more details about the constitutive model, see Refs. 17 and 20.

After the definition of the constitutive model, it is necessary to define the two-bar truss strain in order to allow the use of the constitutive equation in the equilibrium Eq. (1). Hence, by assuming the strain as follows:

$$\varepsilon = \frac{l}{l_0} - 1 = \frac{\cos\varphi_0}{\cos\varphi} - 1 \tag{7}$$

it is possible to obtain the stress, σ, which is used to calculate the external force presented in Eq. (1), $F = \sigma A$. Thus, the equation of motion presented in Eq. (1) may be rewritten as follows:

$$m\ddot{X} + c\dot{X} + 2A\frac{X}{(X^2 + (B + \frac{D}{2})^2)^{1/2}}\left\{E\left[\frac{(X^2 + (B + \frac{D}{2})^2)^{1/2}}{l_0} - 1\right] + [\alpha + E\alpha_h](\beta_2 - \beta_1) - \Omega(T - T_0)\right\} = P(t), \tag{8}$$

where B is the horizontal projection of each truss bar (Fig. 1). Considering a periodic excitation $P = P_0 \sin(\omega t)$ the equation of motion may be written in nondimensional

form as:

$$\begin{aligned} x' &= y \\ y' &= \gamma \sin(\varpi \hat{t}) - \xi y - \mu_E \left[1 - \frac{1}{(x^2 + (b + \frac{d}{2})^2)^{1/2}}\right] \\ &\quad - [(\hat{\alpha} + \mu_E \alpha_h)(\beta_2 - \beta_1) - \hat{\Omega}\mu_\Omega(\theta - \theta_0)] \frac{x}{(x^2 + (b + \frac{d}{2})^2)^{1/2}}, \end{aligned} \tag{9}$$

where

$$\begin{gathered} x = \frac{X}{l}, \quad b = \frac{B}{l_0}, \quad d = \frac{D}{l}, \quad \omega_0^2 = \frac{2E_R A}{m l_0}, \quad \gamma = \frac{P_0}{m l_0 \omega_0^2}, \\ \xi = \frac{c}{m\omega_0}, \quad \hat{t} = \omega_0 t, \quad \varpi = \frac{\omega}{\omega_0}, \quad \theta = \frac{T}{T_M}, \quad \mu_E = \frac{E}{E_R}, \\ \mu_\Omega = \frac{\Omega}{\Omega_R}, \quad \hat{\alpha} = \frac{\alpha}{E_R}, \quad \hat{\Omega} = \frac{\Omega_R T_R}{E_R} \quad \text{and} \quad ()' = \frac{d()}{d\hat{t}}. \end{gathered}$$

From now on, the symbol t will be used to represent the nondimensional time $\hat{t}$.

2.2. *Time-delayed feedback method*

The TDF method was first proposed by Pyragas[25] and deals with a dynamical system modeled by a set of ordinary nonlinear differential equations as follows:

$$\dot{\mathbf{x}}(t) = \mathbf{Q}(\mathbf{x}, t) + \mathbf{B}(\mathbf{x}, t), \tag{10}$$

where t is time, $\mathbf{x}(t) \in \Re^{\mathbf{n}}$ is the state variable vector, $\mathbf{Q}(\mathbf{x}, t) \in \Re^{\mathbf{n}}$ defines the system dynamics, while $\mathbf{B}(\mathbf{x}, t) \in \Re^{\mathbf{n}}$ is associated with the control action. The TDF control law is based on the difference between one time-delayed state and the present state of the system represented by the following equation:

$$\mathbf{B}(\mathbf{x}, t) = \mathbf{K}[\mathbf{x}_\tau - \mathbf{x}], \tag{11}$$

where $\mathbf{K} \in \Re^{\mathbf{n}\times\mathbf{n}}$ is the feedback gain matrix, $\mathbf{x}_\tau = \mathbf{x}(t - \tau)$ are delayed states of the system and τ is the time delay. The UPO stabilization can be achieved by an appropriate choice of $\mathbf{K}$. Note that for any gain defined by $\mathbf{K}$, perturbation of Eq. (11) vanishes when the system is on the UPO since $\mathbf{x}(t - \tau) = \mathbf{x}(t)$ for all m if $\tau = T_i$, where T_i is the periodicity of the ith UPO.

The TDF method is employed as an inspiration of the controller employed in this work. The control action consists of the displacement, D, and its influence on the system's equations of motion can be observed in Eq. (8). The nondimensional perturbation, represented by variable $d = D/l$, is obtained by using information of nondimensional actual and delayed velocities

$$d = K[y_\tau - y]. \tag{12}$$

It should be pointed out that this proposition differs from the TDF usual form since control action is not an independent term as presented in Eq. (10).

The determination of the control gain can be obtained by analyzing the Lyapunov exponents related to the UPO that should be stabilized. De Paula and Savi[1] showed that a proper way to define the controller parameter is to look for values that make the Lyapunov exponent of an UPO negative. In this work, this methodology is not employed and gain is arbitrarily chosen using a trial-error approach.

3. Control the Two-Bar Truss

Numerical simulations are carried out considering an iterative procedure based on the operator split technique,[26] the orthogonal projection algorithm[18] and the classical fourth order Runge–Kutta method. In all simulations, the material properties presented in Table 1, which represent typical values for SMAs, are used. For these data, the parameters defined in Eq. (9) assume the values: $x_0 = 0.4472$, $b = 0.894$, $\omega_0^2 = 1.2 \times 10^{10}$, $\xi = 0$, $\theta = 1.28$, $\hat{\alpha} = 2.78 \times 10^{-3}$, $\hat{\Omega} = 5.11 \times 10^{-3}$.

The uncontrolled forced response of the SMA two-bar truss is initially addressed. This is done by letting d vanish in the equations of motion (9). High temperature behaviors, related to the pseudoelastic effect, are of concern. Savi and Nogueira[12] discussed the general behavior of this structure presenting free and forced vibrations analyses.

In order to start the analysis, the bifurcation diagram is considered representing stroboscopically sampled displacement values, x, under the slow quasi-static increase or decrease of a system parameter. Initially, two situations are considered: in one case the driving frequency, ϖ, is of concern, assuming a fixed forcing amplitude $\gamma = 0.01$; the other situation considers that the forcing amplitude, γ, is varied while $\varpi = 0.3347$. Figure 2 presents these bifurcation diagrams by increasing the forcing frequency (left) and the forcing amplitude (right). Results show regions related to cloud of points and also regions represented by a discrete number of points associated with periodic motions. Differences among distinct forcing parameters values are noticeable. The range of analyzed forcing frequency and amplitude presents distinct kinds of behaviors including periodic and quasi-periodic responses, chaotic behavior and also mutistability related to the coexistence of attractors. A more detailed discussion about the system behavior is presented in Savi and Nogueira.[12]

Table 1. SMA constitutive parameters.

E_A (GPa)	E_M (GPa)	α (MPa)	α_h
54	54	150	0.052
L_0 (MPa)	L (MPa)	(MPa)	L^A (MPa)
0.15	41.5	0.63	185
Ω_A (MPa/K)	Ω_M (MPa/K)	T_M (K)	T_A (K)
0.74	0.17	291.4	307.7
η^L (MPa.s)	η^U (MPa.s)		
10	27		

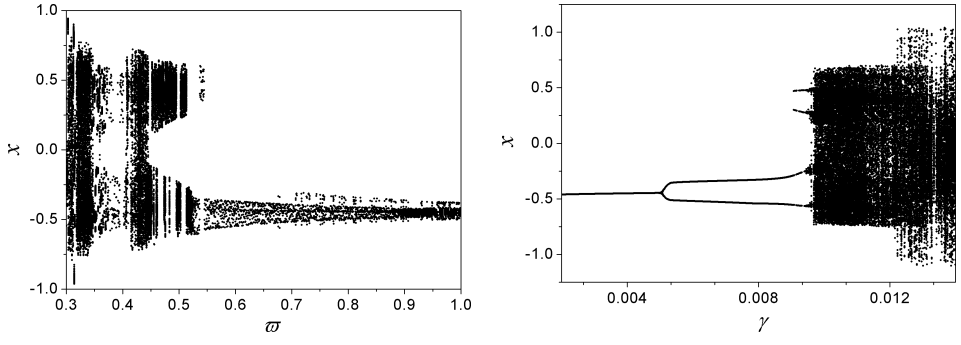

Fig. 2. Bifurcation diagrams. (a) Varying ϖ with $\gamma = 0.01$ and (b) varying γ with $\varpi = 0.3347$.

Some aspects of the system response for a specific set of parameters are now presented. Figure 3 shows phase space together with Poincaré section and volume fraction evolution by considering $\varpi = 0.3347$ and $\gamma = 0.01$. A chaotic-like behavior, related to a typical strange attractor observed in the Poincaré section, is noticeable. This motion is complex, filling both positive and negative sides of phase space and therefore, presenting the snap-through behavior. This complex response is chosen in order to verify the capability of the control technique to reduce system vibration and also to avoid the snap-through behavior. From volume fraction evolution, it is observed that there is austenitic phase, A, close to the stable equilibrium points. In these regions, the truss is free of stress and therefore, austenitic phase is stable since a high temperature is considered. The definition of high temperature corresponds to temperatures higher than T_A, which represents the temperature above which austenite is stable in a stress-free state. When the truss oscillates and goes way from its

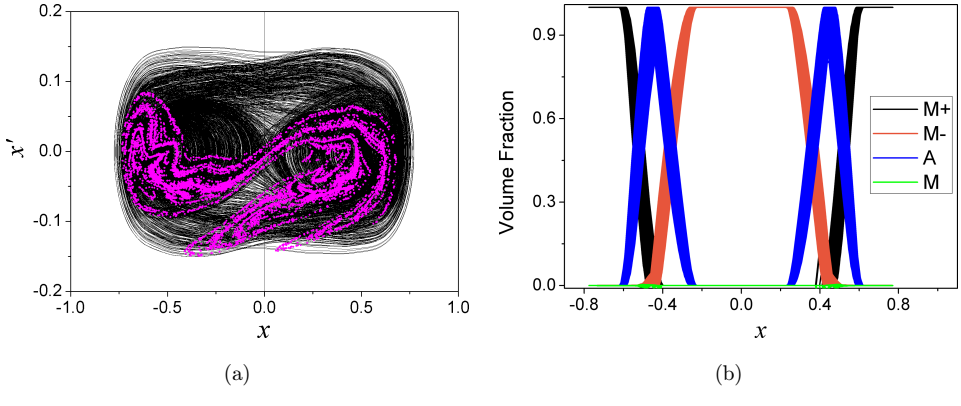

Fig. 3. Response for $\gamma = 0.01$ and $\varpi = 0.3347$. (a) Phase space and Poincaré section showing chaotic-like response and (b) volume fraction–displacement curves.

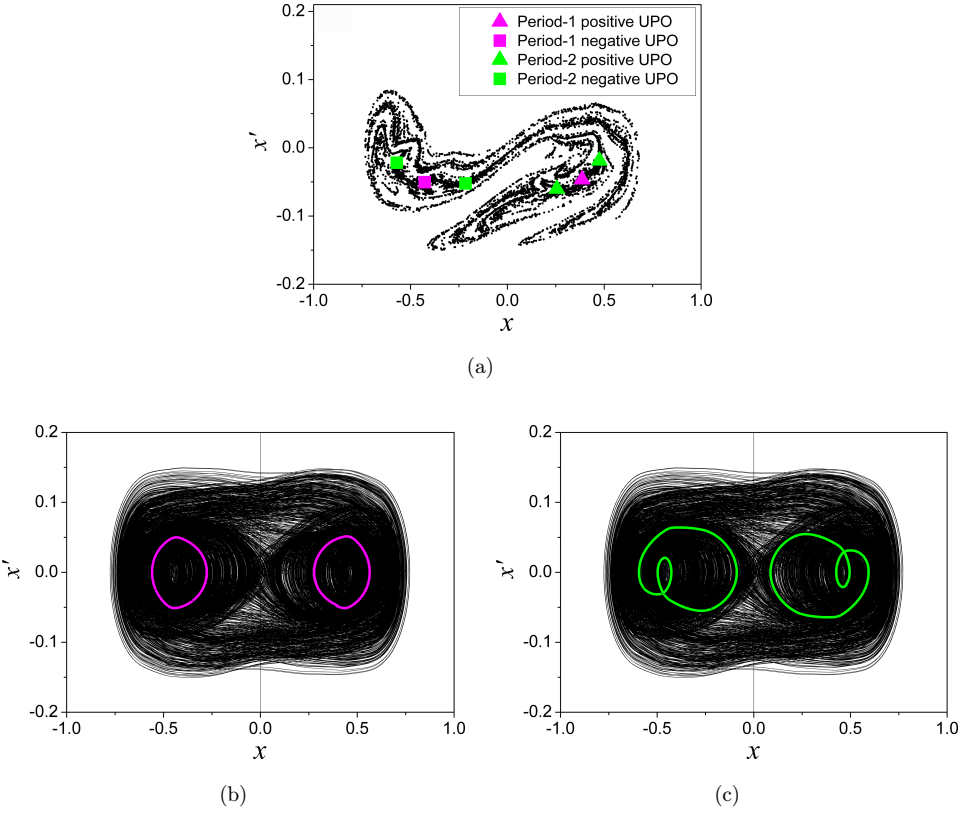

Fig. 4. Identified UPOs. (a) Poincaré section; (b) period-1 UPOs in phase space and (c) period-2 UPOs in phase space.

stable equilibrium points, stress induces martensitic phases, being induced by tensile stress, $M+$, or compressive stress, $M-$.

Chaotic behavior has a structure of UPOs that constitute the essential background of this response. The identification of UPOs embedded in the chaotic attractor is performed using the close return method.[27] Figure 4 shows four identified UPOs both in Poincaré section and phase space plots. Note that each one is restricted to only one side of the phase plane, called half-phase plane, that would be positive or negative, respectively related to positive or negative displacements. This means that snap-through behavior does not occur in a specific UPO since no jumps are observed.

After these considerations about the uncontrolled behavior of the system, controlled situations are of concern. Initially, the period-1 UPO stabilization is of treated. Figure 5 presents the response of the controlled system for $\tau = 1$ and $K = 1$. Note that the controller stabilizes the negative period-1 UPO. Figure 5 shows the time history of the system displacement and of the control perturbation, the

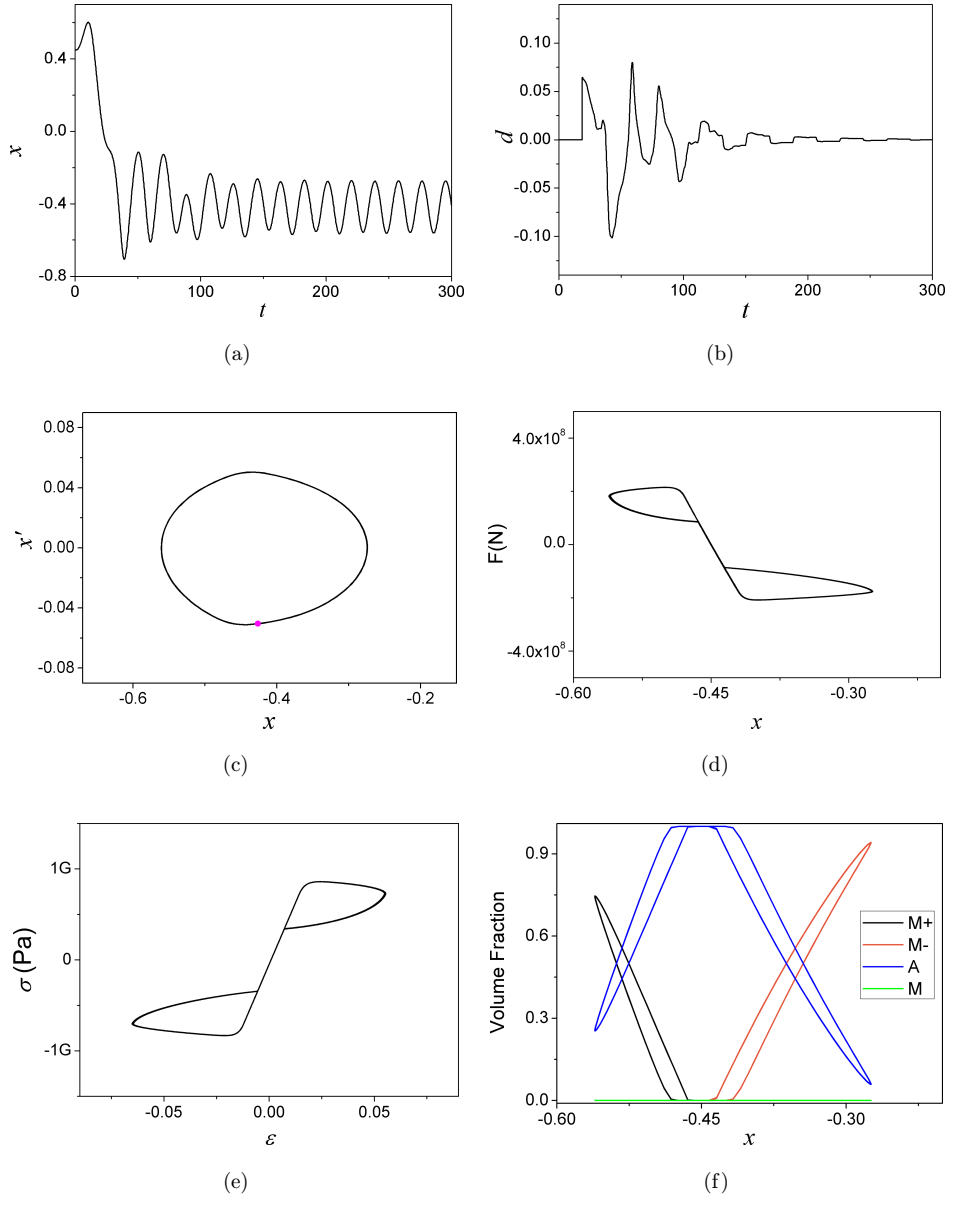

Fig. 5. Positive period-1 UPO stabilized with $\tau = 1$ and $K = 1$. (a) System displacement; (b) control action; (c) stabilized orbit in phase space; (d) force–displacement curve; (e) stress–strain diagram and (f) volume fraction–displacement curves.

stabilized orbit in phase space, the force–displacement curve, the stress–strain diagram and the volume fraction–displacement curves.

Figure 6 shows the same results related to the stabilization of the other period-1 UPO identified in Fig. 4. This stabilization is achieved considering the same control

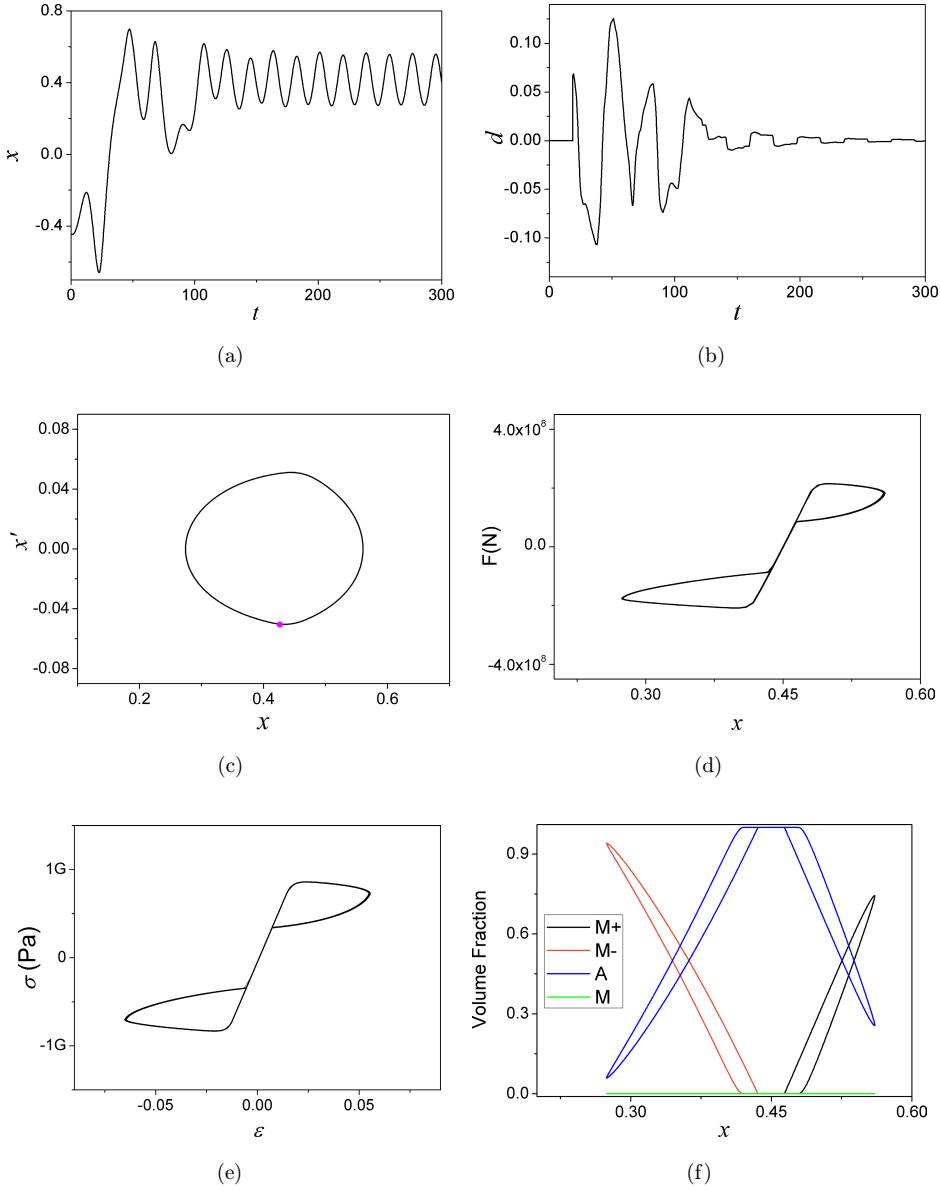

Fig. 6. Negative period-1 UPO stabilized with $\tau = 1$ and $K = 1$, assuming control action as $-d$. (a) System displacement; (b) control action; (c) stabilized orbit in phase space; (d) force–displacement curve; (e) stress–strain diagram and (f) volume fraction–displacement curves.

parameters of the previous case, but assuming the control action as $-d$. It should be noticed the asymmetric characteristic of the force–displacement curve. It is important to highlight that these stabilizations avoid critical vibration situations including the snap-through behavior.

The stabilization of the period-2 UPO is considered by assuming $\tau = 2$. Figure 7 presents the controlled system response for $K = 0.7$. Once again, the controller is able to stabilize a desired UPO, avoiding critical vibrations. In contrast with Figs. 5, 6(a) and 6(b), where all time history response and control action were shown,

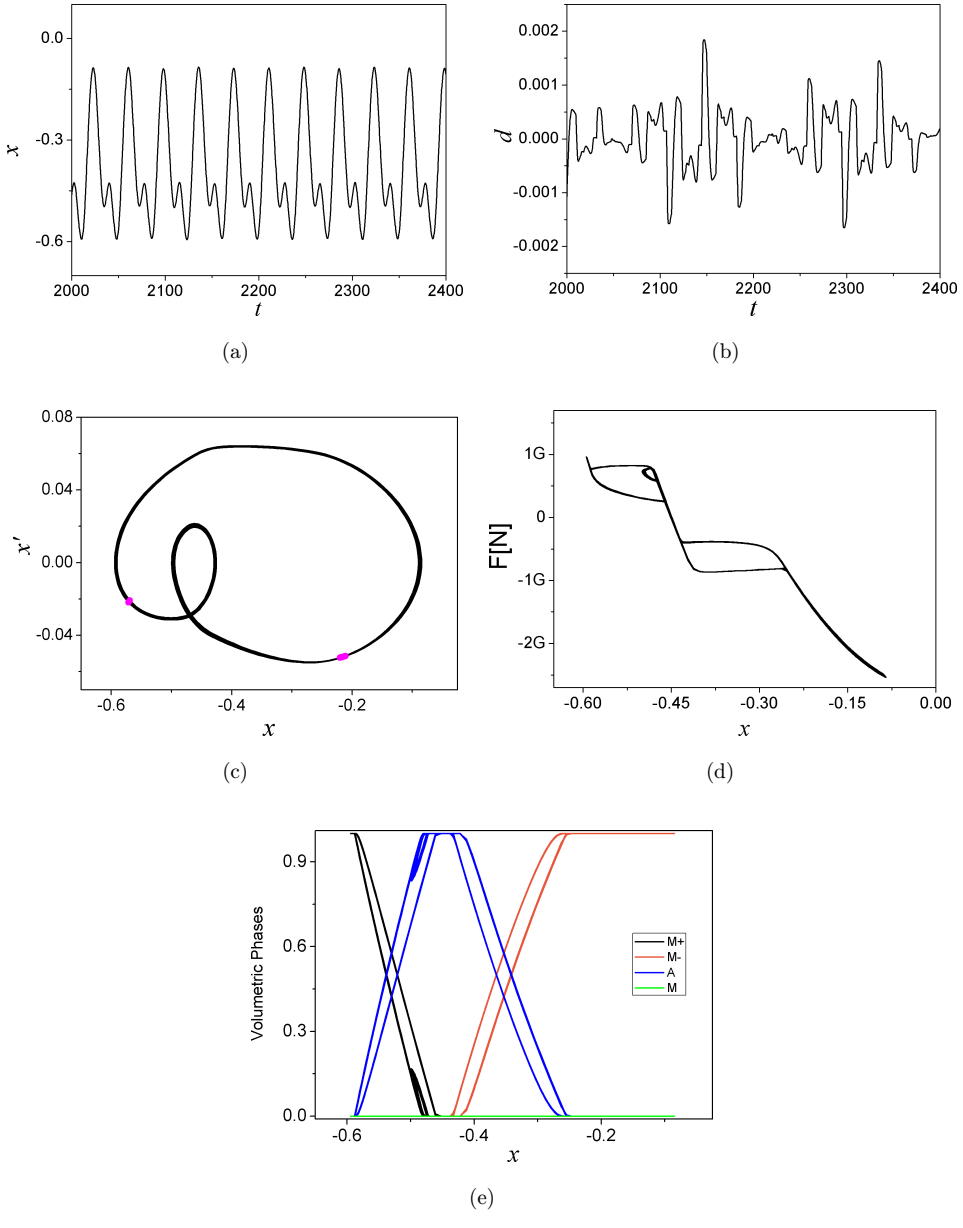

Fig. 7. Period-2 UPO stabilized with $\tau = 2$ and $K = 0.7$. (a) System displacement; (b) control action; (c) stabilized orbit in phase space; (d) force–displacement curve and (e) volume fraction–displacement curves.

Figs. 7(a) and 7(b) present only steady state response once the transient is longer in this case.

4. Bifurcation Control

In this section, chaos control is employed for bifurcation control purposes as proposed by De Paula *et al.*[28] Therefore, the TDF is employed not only at fixed values of forcing frequency and amplitude but also when the forcing parameters are varying. As for instance, since a period-1 UPO showed in Fig. 8 provides acceptable oscillation amplitudes, the objective now is to retain it, even with time varying forcing parameters.

Initially, the increase of the forcing frequency is considered with a constant forcing amplitude $\gamma = 0.01$. Figure 8 shows uncontrolled bifurcation diagram together with controlled one where control action employs $\tau = 1$ and $K = 1$. The control gain is the same used to stabilize the period-1 UPO previously analyzed once this is the desired orbit. Note that the TDF is able to stabilize a period-1 UPO in all range of analyzed forcing frequency, avoiding the bifurcation. It is important to highlight that the same gain, $K = 1$, is used for all forcing frequencies. Figure 9 shows the time history of the control action when the bifurcation diagram control starts. Note that, initially, a control effort is necessary to stabilize the UPO. After the stabilization is achieved the control action vanishes until the forcing frequency has its first variation, that occurs at $t = 950$. At this point, a control action is necessary again in order to overcome the perturbation and maintain the UPO stable. After the stabilization, the control action vanishes again, until the next variation in the forcing frequency, as it can be observed in Fig. 9. Note that the control effort when control starts is higher than when forcing frequency is varied. This happens because the initial system trajectory is not in the neighborhood of the desired UPO.

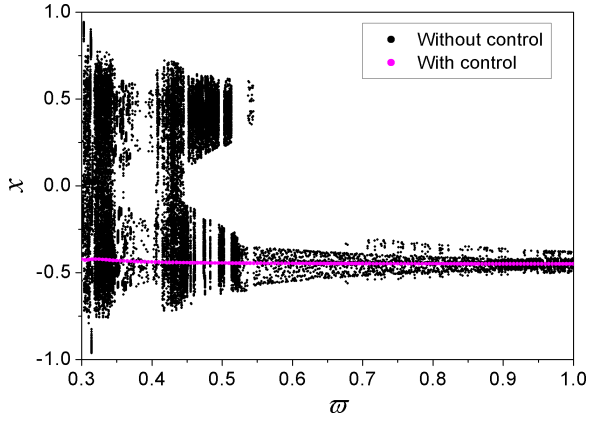

Fig. 8. Bifurcation diagram increasing forcing frequency when $\gamma = 0.01$ without control action and with control action for $\tau = 1$ and $K = 1$.

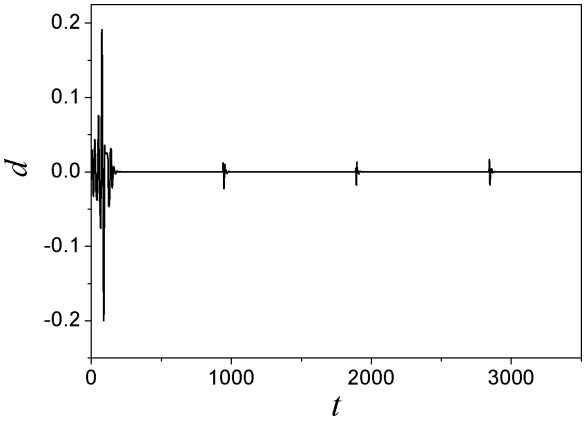

Fig. 9. Control action when bifurcation diagram control starts.

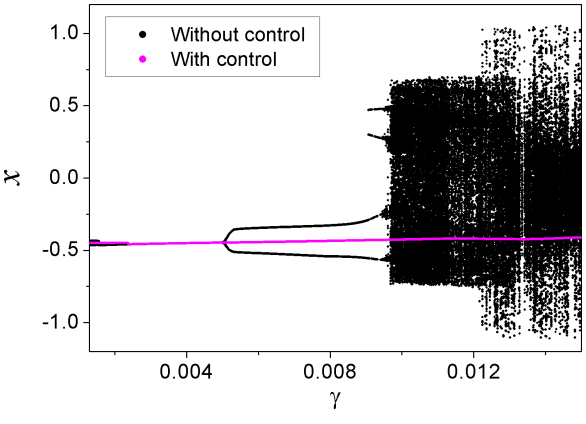

Fig. 10. Bifurcation diagram increasing forcing amplitude when $\varpi = 0.3347$ without control action and with control action for $\tau = 1$ and $K = 1$.

The increase of the forcing amplitude is of now of concern for a specific frequency, $\varpi = 0.3347$. Figure 10 shows uncontrolled bifurcation diagram together with controlled response where control action are defined for $\tau = 1$ and $K = 1$. Once again, considering the same control gain, the TDF is able to stabilize the period-1 UPO and avoid bifurcation in all range of analyzed forcing amplitude.

5. Conclusion

This article reports results from numerical simulations of chaos control of an SMA two-bar truss. This system represents an archetypal model useful for the stability investigation of adaptive trusses with shape memory alloy actuators. A constitutive model with internal constraints is assumed to describe the thermomechanical

behavior of the bars. An iterative numerical procedure based on the operator split technique, the orthogonal projection algorithm and the classical fourth order Runge–Kutta method is developed to deal with nonlinearities in the formulation. A continuous chaos control method, time delayed feedback, is employed to stabilize unstable periodic orbits embedded in chaotic attractor. This approach is useful for vibration reduction, avoiding snap-through behavior. Moreover, the approach is useful for bifurcation control purposes. By considering forcing frequency amplitude and frequency variations, the controller is able to sustain a desired UPO, avoiding bifurcations. Therefore, the chaos control approach is interesting for different purposes, promoting vibration reduction, avoiding snap-through behavior, stabilizing desired UPOs and also controlling bifurcations.

Acknowledgments

The authors would like to acknowledge the support of the Brazilian Research Agencies CNPq, CAPES and FAPERJ and through the INCT-EIE (National Institute of Science and Technology — Smart Structures in Engineering) the CNPq and FAPEMIG. The AFOSR (Air Force Office of Scientific Research) is also acknowledged.

References

1. A. S. de Paula and M. A. Savi, Controlling chaos in a nonlinear pendulum using an extended time-delayed feedback control method, *Chaos, Solitons Fractals* **42**(5) (2009) 2981–2988.
2. A. S. de Paula and M. A. Savi, Comparative analysis of chaos control methods: A mechanical system case study, *Int. J. Nonlinear Mech.* **46**(8) (2011) 1076–1089.
3. Z. P. Bazant and L. Cedolin, *Stability of Structures* (Oxford Press, New York, 1991).
4. I. Ario, Homoclinic bifurcation and chaos attractor in elastic two-bar truss, *Int. J. Nonlinear Mech.* **39** (2004) 605–617.
5. M. Tada and A. Suito, Static and dynamic post-buckling behavior of truss structures, *Eng. Struct.* **20**(4–6) (1998) 384–389.
6. P. B. Gonçalves and Z. J. G. N. Del Prado, Nonlinear oscillations and stability of parametrically excited cylindrical shells, *Meccanica* **37** (2002) 569–597.
7. M. S. Soliman and P. B. Gonçalves, Chaotic behavior resulting in transient and steady state instabilities of pressure-loaded shallow spherical shells, *J. Sound Vibr.* **259**(3) (2003) 497–512.
8. G. Parry, J. Colin, C. Coupeau, F. Foucher, A. Cimetière and J. Grilhé, Snapthrough occurring in the postbuckling of thin films, *Appl. Phys. Lett.* **86** (2005) 081905.
9. S. Choi, J. J. Lee, D. C. Seo and S. W. Choi, The active buckling control of laminated composite beams with embedded shape memory alloy wires, *Composite Struct.* **47** (1999) 679–686.
10. D. Z. Yankelevsky, Elastic-plastic behavior of a shallow two bar truss, *Int. J. Mech. Sci.* **41** (1999) 663–675.
11. M. A. Savi, P. M. C. L. Pacheco and A. M. B. Braga, Chaos in a shape memory two-bar truss, *Int. J. Nonlinear Mech.* **37**(8) (2002) 1387–1395.
12. M. A. Savi and J. B. Nogueira, Nonlinear dynamics and chaos in a pseudoelastic two-bar truss, *Smart Mater. Struct.* **19**(11) Article 1150222010 (2010) 1–11.

13. W. M. Bessa, A. S. de Paula and M. A. Savi, Adaptive fuzzy sliding mode control of smart structures, *Eur. Phys. J. — Special Topics* **222**(7) (2013) 1541–1551.
14. D. C. Lagoudas, *Shape Memory Alloys: Modeling and Engineering Applications* (Springer, New York, 2008).
15. A. Paiva and M. A. Savi, An overview of constitutive models for shape memory alloys, *Math. Problems Eng.* **2006**, Article ID56876 (2006) 1–30.
16. L. G. Machado and M. A. Savi, Medical applications of shape memory alloys, *Braz. J, Med. Biol. Res.* **36**(6) (2003) 683–691.
17. A. Paiva, M. A. Savi, A. M. B. Braga and P. M. C. L. Pacheco, A constitutive model for shape memory alloys considering tensile-compressive asymmetry and plasticity, *Int. J. Solids Struct.* **42**(11–12) (2005) 3439–3457.
18. M. A. Savi, A. Paiva, A. P. Baêta-Neves and P. M. C. L. Pacheco, Phenomenological modeling and numerical simulation of shape memory alloys: A thermo-plastic-phase transformation coupled model, *J. Intell. Mater. Syst. Struct.* **13**(5) (2002) 261–273.
19. A. P. Baêta-Neves, M. A. Savi and P. M. C. L. Pacheco, On the Fremond's constitutive model for shape memory alloys, *Mech. Res. Commun.* **31**(6) (2004) 677–688.
20. M. A. Savi and A. Paiva, Describing internal subloops due to incomplete phase transformations in shape memory alloys, *Arch. Appl. Mech.* **74**(9) (2005) 637–647.
21. P. C. C. Monteiro Jr., M. A. Savi, T. A. Netto and P. M. C. L. Pacheco, A phenomenological description of the thermomechanical coupling and the rate-dependent behavior of shape memory alloys, *J. Intell. Mater. Syst. Struct.* **20**(14) (2009) 1675–1687.
22. R. A. A. Aguiar, M. A. Savi and P. M. C. L. Pacheco, Experimental and numerical investigations of shape memory alloy helical springs, *Smart Mater. Struct.* **19**(2) (2010) 025008, 1–9.
23. S. A. Oliveira, M. A. Savi and A. L. Kalamkarov, A three-dimensional constitutive model for shape memory alloys, *Arch. Appl. Mech.* **80**(10) (2010) 1163–1175.
24. R. T. Rockafellar, *Convex Analysis* (Princeton Press, 1970).
25. K. Pyragas, Continuous control of chaos by self-controlling feedback, *Phys. Lett. A* **170** (1992) 421–428.
26. M. Ortiz, P. M. Pinsky and R. L. Taylor, Operator split methods for the numerical solution of the elastoplastic dynamic problem, *Comput. Meth. Appl. Mech. Eng.* **39** (1983) 137–157.
27. D. Auerbach, P. Cvitanovic, J.-P. Eckmann, G. Gunaratne and I. Procaccia, Exploring chaotic motion through periodic orbits, *Phys. Rev. Lett.* **58**(23) (1987) 2387–2389.
28. A. S. De Paula, M. A. Savi, M. Wiercigroch and E. Pavlovskaia, Bifurcation control of a parametric pendulum, *Int. J. Bifurcation Chaos* **22**(5) (2012) Article 1250111, 1–14.